Proceedings of the IGTI:
ASME TURBO EXPO 2000
8-11 May 2000
Munich, Germany

2000-GT-0446

THE EFFECT OF AIRFOIL SCALING ON THE PREDICTED UNSTEADY LOADING ON THE BLADE OF A 1 AND 1/2 STAGE TRANSONIC TURBINE AND A COMPARISON WITH EXPERIMENTAL RESULTS

J. P. Clark, G. M. Stetson,
S. S. Magge, and R. H. Ni
United Technologies Pratt & Whitney
400 Main St., M/S 201-09
East Hartford, CT 06108

C. W. Haldeman, Jr. and M. G. Dunn
Gas Turbine Laboratory
Ohio State University
2300 West Case Road
Columbus, OH 43235

ABSTRACT

In this study, two time-accurate Navier-Stokes analyses were obtained to predict the first-vane/first-blade interaction in a 1 and 1/2-stage turbine rig for comparison with measurements. In the first computation, airfoil scaling was applied to the turbine blade to achieve periodicity in the circumferential direction while modeling 1/18 of the annulus. In the second, 1/4 of the wheel was modeled without the use of airfoil scaling. For both simulations the predicted unsteady pressures on the blade were similar in terms of time-averaged pressure distributions and peak-peak unsteady pressure envelopes. However, closer inspection of the predictions in the frequency domain revealed significant differences in the magnitudes of unsteadiness at twice vane-passing frequency (and the vane-passing frequency itself, to a lesser extent). The results of both computations were compared to measurements of the vane-blade interaction in a full-scale turbine rig representative of an early design iteration of the PW6000 engine. These measurements were made in the short-duration turbine-test facility at The Ohio State University Gas Turbine Laboratory. The experimentally determined, time-resolved pressures were in good agreement with those predicted with the 1/4-wheel simulation.

INTRODUCTION

Periodic unsteadiness is inherent to flows in gas turbine engines. Sharma et al. (1992) have reviewed and assessed both computational (e.g. Rai, 1987, Giles, 1988) and experimental research activities (e.g. Dring et al., 1982) in the field of unsteady flows in turbomachines. They noted that certain phenomena, such as the segregation of relatively hotter and cooler gases to the pressure and suction sides, respectively, of rotor airfoils could be predicted by time-accurate analysis of rotor-stator interaction in the presence of circumferential distortions in turbine inlet-temperature. Consequently, Sharma and his co-workers called for the further improvement of computational techniques such that designers could incorporate time-accurate analyses into the design process to make timely decisions. Since that time, developments in predictive methods such as multi-grid techniques and implicit dual time-stepping, coupled with parallelization of codes, have made this possible (Ni, 1999). Designers can now execute 3-D, unsteady Navier-Stokes analyses to predict the periodic-unsteady forcing function required to calculate resonant stresses in multi-row, transonic turbines (Hilbert et al., 1997) and make design changes, as necessary.

Experimental techniques to elucidate the physical mechanisms involved in unsteady flows have also continued to evolve since the review article of Sharma et al. In particular, much use has been made of short-duration facilities like that described by Jones et al., 1973 that are capable of reproducing the corrected mass flows, corrected speeds, Reynolds numbers, and gas-to-wall temperature ratios associated with modern transonic turbines. Such experiments have been used to assess the ability of state-of-the-art codes to predict both the time-averaged and time-resolved pressure loadings on transonic airfoils (e.g. Rao et al., 1994, and Hilditch et al., 1998). In the study of Busby et al., 1998, four separate Reynolds-Averaged Navier-Stokes numerical procedures (2D as well as 3D codes) were used to predict the unsteady pressure fluctuations in a single-stage transonic turbine. It was found that all four schemes were in general agreement with one another and compared well with time-resolved measurements.

The turbine stage in the study of Busby et al. was designed for spatial periodicity on 24 degrees of the annulus, and this made 3D, time-accurate modeling of the stage relatively straightforward. In practice, a turbine designer deals with airfoil rows of arbitrary count, and often, circumferential periodicity exists only on a much larger portion of the annulus. To reduce the computational complexity of a

3D multi-row, unsteady aerodynamic analysis of a gas turbine, the airfoil count in one (or more) of the rows is commonly altered and the airfoils in that row are scaled such that the airfoil pressure distributions are held approximately constant (e.g. Rai, 1987, and Rai and Madavan, 1990). Such scaling is sometimes imperative to make time-accurate analysis feasible during the design process where decisions must often be made to reduce levels of periodic unsteadiness and resonant stresses. Although it is well known that the tonal acoustics of rotor-stator interaction are dependent upon the airfoil count (e.g. Tyler and Sofrin, 1970, and Rangwalla and Rai, 1993), a turbine-airfoil designer must often act upon the results of a scaled analysis. When a designer bases decisions on results from a scaled analysis, he assumes tacitly that the only effect of scaling is to shift the frequencies of excitation. That is, he presumes that the magnitude and phase of the unsteadiness are unaffected. Here, the effect of such airfoil scaling on the predicted flowfield in a 1 and 1/2 stage transonic turbine is studied with a time-accurate 3D Navier-Stokes solver, and the results are compared with experimental data.

THE TURBINE MODEL AND EXPERIMENTAL TECHNIQUE

In this study, the short-duration turbine-test facility at the Gas Turbine Laboratory of the Ohio State University was used to measure the time-averaged and time-resolved surface pressures on airfoils in a full-scale, 1 and 1/2 stage transonic turbine. The turbine rig (See Fig. 1 and Table 1) was representative of an early design iteration of the PW6000 engine, which is currently under development. The airfoil counts of the model were 36:56:36 in the first vane, first blade, and second vane rows, respectively. The transient facility at OSU, which has been described thoroughly by Dunn et al. (1989), was designed to operate as a reflected-shock tunnel, but may also be utilized as a blowdown facility. For this series of experiments, the facility was operated in both modes. However, it was noted that, during the transient test-time, the inlet flow conditions obtained in blowdown mode were steadier than those measured in reflected-shock mode. Since the intent of the experiments was to assess the predictive capabilities of an in-house CFD code at Pratt & Whitney that assumes steady upstream conditions, the time-resolved aerodynamic results presented here were collected when the tunnel was operated in blowdown mode only.

Prior to a tunnel blowdown run, both the driver and driven sections of the shock-tube were filled with air at the same high-pressure (and room temperature) and no diaphragms were used to separate the sections. Therefore, the entire length of the shock tube acted as the driver section of the blowdown runs. Meanwhile, the turbine, which was situated in near-vacuum conditions in the facility dump tank and separated from the driver and driven sections of the tube by a fast-acting valve, was brought to somewhat less than the design speed with an air motor.

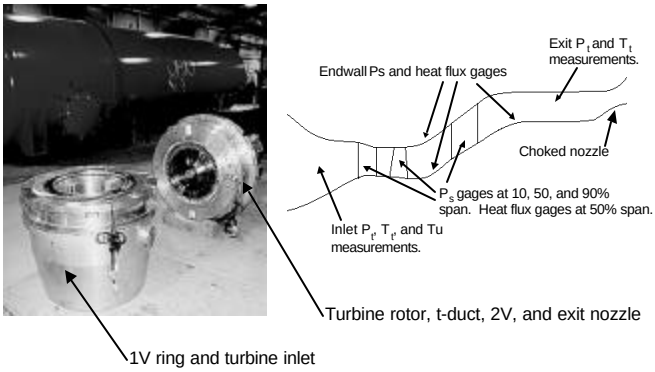

Figure 1. The 1+1/2 stage transonic turbine tested at OSU for this study was heavily instrumented on airfoils in each row and along the rig flowpath.

At the start of a run, the fast-acting valve was opened, and a starting shock was swallowed by the divergent section of a de Laval nozzle until it came to rest as a normal shock just upstream of the turbine-model inlet. The compression-heating associated with the moving shock, total-pressure drop across it, and the increase in wheel speed of the turbine due to work extraction from the flow during the run were all predictable and repeatable. Consequently, the driver pressure, the position of the turbine inlet in the divergent portion of the de Laval nozzle, and the initial wheel speed were all set to achieve the design flow parameter and speed parameter during the run. Additionally, altering the throat area of a choked nozzle downstream of the turbine allowed for the pressure-ratio across the turbine model to be adjusted. During the approximately 100ms run-time of the facility, the upstream area-averaged total pressure and the wheel speed were approximately constant, varying by 8 and 0.6%, respectively over the 40ms interval of data reduced here for a given tunnel run. Both

NOMENCLATURE

b_x = airfoil axial chord (cm)
E = engine order or nondimensional frequency of excitation (60 f / N)
f = frequency of excitation (Hz)
DFT = Discrete Fourier Transform
N = wheel speed (rpm)
p = fluctuating pressure (Pa)
P,P_s = static pressure (Pa)
P_t = total pressure (Pa)
Pt,in = inlet total pressure (Pa)
PSD = Power-Spectral Density
r = radial distance (cm)
t = time (s)
T_t = total temperature (K)
Tu = turbulence intensity (%)
U = rotor tangential velocity (m/s)
x = axial distance (cm)
y^+ = non-dimensional distance (law-of-the-wall variable)
1B = first blade
1V = first vane
2V = second vane
36E = engine order of vane-passing frequency
72E = engine order of twice vane-passing frequency
Δt = interval between samples (s)
τ_{rev} = period of rotor revolution (s)
τ_{vp} = period of vane passing (s)

time-resolved static and total pressures were recorded, and instantaneous static-to-total pressure ratios were formed before subsequent data reduction to mitigate the effects of the time-varying upstream total conditions.

As seen in Fig. 1, which contains both a photograph of the model and a schematic of its flowpath, the turbine was heavily instrumented both on the airfoils and along the endwalls with flush-mounted Kulite piezo-resistive pressure transducers and thin-film heat flux gages. Total pressures and temperatures were measured on upstream rakes and a downstream traverse. Also, the leading edge of an upstream circular cylinder was instrumented with heat-flux gages to infer the inlet turbulence-intensity from measurements of the stagnation-point Frossling number (Smith and Kuethe, 1966). The turbulence intensity was estimated to be 7+/-3%, but no inlet turbulence was modeled in the simulations described in the next section.

The main objective of this work is to assess the capability of in-house codes at Pratt & Whitney to predict unsteady forcing functions on blades in transonic turbines. So, what follows primarily concerns the time-resolved pressure measurements on the first blade of the turbine model at 10, 50, 69, and 90%. For each tunnel run, all unsteady pressures were sampled simultaneously at 100kHz using a 12-bit data-acquisition system. Each transducer had an active sensing area of 0.64mm by 0.64mm, and all sensors were calibrated throughout the entire data system at regular intervals during the test program. Further details of the calibration technique and typical results were reported by Dunn and Haldeman (1995).

COMPUTATIONAL METHODS

The time-mean and time-resolved unsteady pressure fields in the 1 and 1/2 stage transonic turbine were predicted using the 3-D, multi-stage Reynolds-Averaged Navier-Stokes code described collectively by Ni (1982), Ni and Bogoian (1989), and Davis et al. (1996). The code employs implicit dual time-stepping to solve for the periodic-unsteady flowfield on an H-grid, and numerical closure is obtained via the Baldwin-Lomax (1978) turbulence model. The code is accurate to second-order in space and time. Both local time-stepping and multi-grid techniques are used with a finite-volume, cell-vertex-centered Lax-Wendroff (1964) method for each inner sub-iteration to obtain rapid convergence. For time-accurate calculations of rotor/stator-interaction with the Ni code, the flowfield is solved on a portion of the annulus over which spatial periodicity occurs.

For the model turbine of this study, with airfoil counts of 36:56:36, circumferential periodicity occurred on 1/4 of the wheel, so a time-accurate solution of the 3-D flowfield required a model having airfoil counts of 9:14:9, as seen in Table 1. The grid counts used for each airfoil passage are also listed in the table, and these are consistent with grids used during the design process at P&W. The P&W design viscous-grid provides values of y^+ less than 5 over all airfoil surfaces as recommended by Dunham and Meauze (1998) for use with mixing-length turbulence models. Also, the grid gives approximately 10 grid points in the boundary layer on each airfoil surface and 20 grid points in the wakes near the airfoil trailing edges.

Note that the total number of grid points needed for the 1/4-wheel model was in excess of 12.3 million. However, if a modicum of blade scaling was used (See Fig. 2 and Table 1), and the airfoil counts were changed to 36:54:36, a 2:3:2 model could be employed over 1/18 of the annulus. For the same grid density, less than 2.7 million grid points were required. This was a considerable reduction in computational resources, and such scaling was utilized during the design phase of the rig and to decide the placement of sensors on the turbine surfaces.

Mainflow Conditions :	Design		Measured
Pt,inlet / Ps.exit	5.19		5.17
Speed Parameter (rpm / $K^{1/2}$)	421		419
Inlet Flow Parameter (kg $K^{1/2}$) / (Pa s)	$7.69x10^{-4}$		N/A
Model Geometry :	1V	1B	2V
Airfoils Per Row	36	56	36
Mean Radius (cm)	29.21	28.98	32.99
Mid-span Axial Chord (cm)	3.07	2.54	5.08
Inlet Mach No. (isentropic)	0.10	0.28	0.48
Exit Mach No. (isentropic)	0.92	1.17	0.71
CFD Models :	1V	1B	2V
Number of Airfoils (1/4 Wheel)	9	14	9
Grid Counts	97x49x57	145x49x57*	161x49x57
Total Number of Grid Points :	*$>12.3x10^6$*		
Number of Airfoils (1/18 Wheel)	2 (36)	3 (54)	9 (36)
Grid Counts	97x49x57	145x49x57*	161x49x57
Total Number of Grid Points :	*$< 2.7x10^6$*		

* Each blade also had a 55x16x16 Tip-Clearance Grid

Table 1. Rig operating conditions, geometric definitions, and details of the time-accurate simulations.

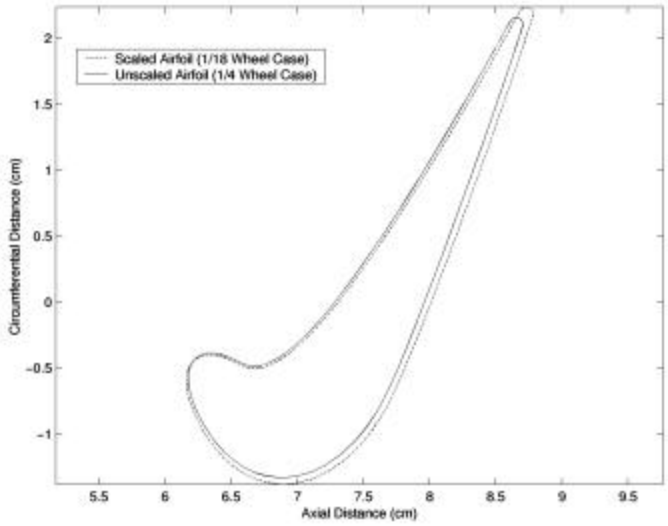

Figure 2. Mid-span blade geometries for the 1/4-wheel and 1/18-wheel simulations.

Since the turbine rig described above was modeled both with and without the use of blade scaling, this combined experimental/computational study provides a unique database with which to examine the effect of scaling on predicted unsteady pressures. To bring each simulation to convergence, the global time-step was set such that the Nyquist frequency was approximately 500kHz, and the solutions were post-processed in a way that mimicked the experiment. That is, the CFD solution was "sampled" at a data rate

of approximately 100kHz (i.e. 50kHz Nyquist frequency). For the unscaled blade, the time-history of 1/4-revolution was recorded, and this was compared to 4 global cycles of the 1/18-wheel case. In this way, the time-resolved pressures from each case had comparable spectral resolutions, and both spectral-leakage and picket-fencing effects were avoided in the frequency domain.

TIME-MEAN BLADE LOADINGS

Prior to the experimental program, predictions of the unsteady flowfield in the rig were made at design conditions. That is, the simulation results to follow represent true pre-test predictions. The geometry of each of the 36 vanes in the IGV row was measured, and then the average airfoil was modeled for each vane in the prediction. Similarly, each blade was assumed to have the mean shape of four measured airfoils, and the design-intent flowpath and second vanes were simulated. Both the 1/4-wheel and 1/18-wheel simulations were executed prior to the test program. For the 1/18-wheel simulation, the scaled airfoil was shifted axially to hold the 1V-1B midspan axial gap, and the 1V inlet flow parameter (and hence inlet Reynolds number) was also kept constant. The predicted unsteady envelopes for each airfoil were in excellent agreement, and Fig. 3(a)-3(c) are plots of such envelopes for 10, 50, and 90% span on the 1B, respectively. The 1/4-wheel and 1/18-wheel predictions are in very good agreement. This gives some credence to the idea that minimal airfoil scaling such as that used in the 1/18-wheel simulation yields adequate predicted levels of unsteadiness.

The predictions in Fig. 3 are also compared with the peak-to-peak variations and time means of ensemble-averaged experimental pressures. In general, the unsteady envelopes compare well with the predicted peak-to-peak levels. This means that the unsteady interaction with the average vane is well predicted. However, the time-mean blade loading measured in the experiment is not in as good agreement with the prediction for the average blade. Again, only 4 blades out of 56 were used to define the CFD model. Also, there is some apparent unloading of the blade at 90% span. Upon further examination of the sensor logs for the experimental program, it was found that calibration difficulties were experienced for the Kulite at 30% axial chord on the blade suction side. Consequently, systematic

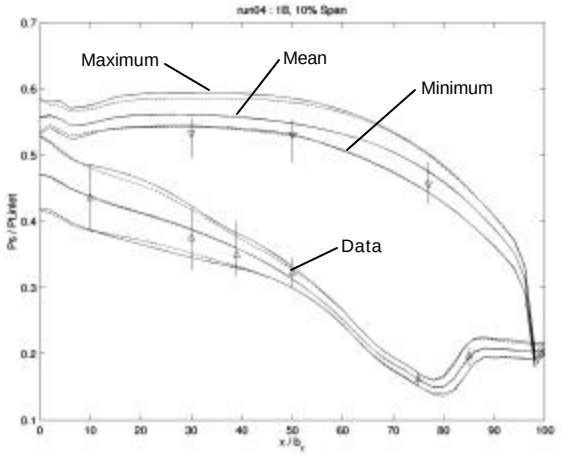

3(a)

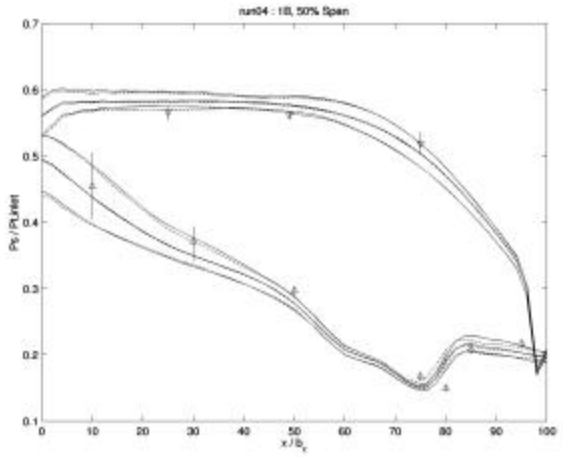

3(b)

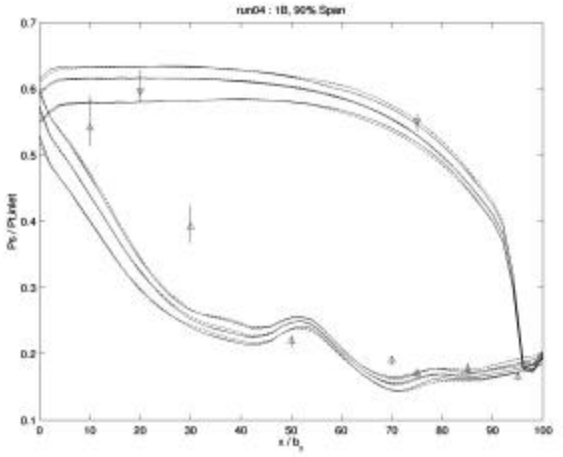

3(c)

Figure 3. Unsteady envelopes for the 1/4-wheel (solid lines) and 1/18-wheel simulations (broken lines) at (a) 10, (b) 50, and (c) 90% span on the 1B.

errors are suspected for that sensor, and the data is only plotted for completeness. This leaves just the data from the sensor at 10% axial chord, which is not enough upon which to make a judgement regarding the efficacy of the tip-clearance modeling in the code, for example. Overall the loadings on all airfoils responded as predicted for changes in incidence and pressure ratio. Moreover, the goal of the study is to assess the predictive capabilities of the Ni code for unsteady forcing functions, and further discussion and analysis is restricted to time-resolved pressures.

TIME-RESOLVED SURFACE PRESSURES

As noted above, all airfoils are identical in the simulations. However, passage-to-passage variations exist in the experiment due to variations necessarily result in discrepancies between the predicted and measured time-resolved pressures. As an example, the unsteadiness

on the blade upstream of the cross-passage shock is primarily a consequence of the blade passing though the circumferential distortion in static pressure associated with each upstream airfoil. Each airfoil around the first vane row was found to have a throat area that was normally distributed about the mean value, so the circumferential variation in static pressure downstream of each vane also varied. Consequently, the time-resolved pressure measured at a fixed location on the blade as it makes one revolution behind the vane row should be different from that predicted in two obvious ways. First, the peak-to-peak level of unsteadiness should be greater than that associated with a vane ring composed of identical airfoils. Second, random unsteadiness should be discernible in the measured traces, but not in the predicted ones.

Figure 4 is a set of 4 normalized pressure traces associated with the Kulite sensor at 77% axial chord on the 1B pressure side at 10% span. In Fig. 4(a), the measured time-resolved pressure is plotted for one quarter of the revolution of the rotor, while in Fig. 4(b) the trace predicted by the 1/4-wheel simulation is shown along with a pair of post-processed experimental traces. Note that the peak-to-peak variation in pressure is greater in the raw experimental data than for the prediction, and the unsteadiness is composed of a broader band of frequencies. It is useful, however, to compare the prediction to a measurement of the unsteadiness due to the average vane.

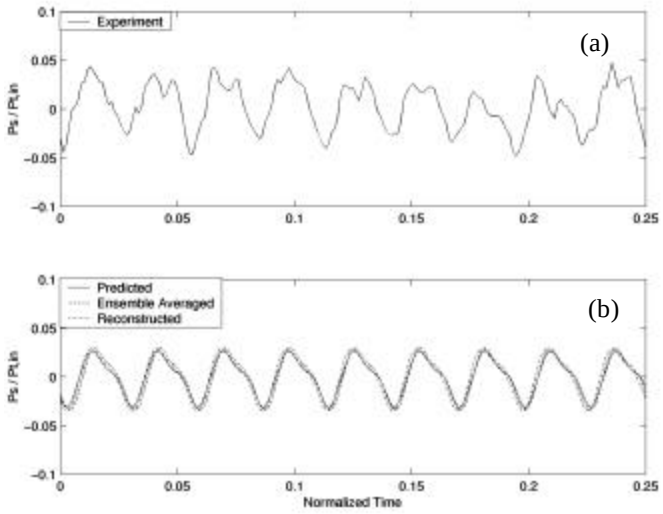

Figure 4. Time-resolved static pressure traces (normalized by upstream total pressure) for a sensor at 10% span and 77% chord on the 1B pressure side. Time is normalized by the period of revolution of the rotor. (a) raw signal, (b) predicted, ensemble-averaged, and reconstructed signals.

It is possible to reconstitute the periodic-unsteady portion of the signal from the raw trace of Fig. 4(a) in one of two ways. Either an ensemble average of the unsteadiness due to each of the 36 vanes is calculated over an integer number of rotor revolutions, or the 36E Fourier components of the measured signal and its harmonics are translated back to the time domain and summed. The results of both of these procedures are plotted in Fig. 4(b), and the traces compare very well with the pressure trace predicted for the average vane in terms of both frequency content and peak-to-peak magnitude. Note that there are small differences in phase between the predicted signal and both the ensemble-averaged and reconstructed experimental traces. This is a consequence of discrepancies between the location of the turbine wheel in the experiment and the prediction. Both the experiment and the prediction were sampled at the same data rate (100kHz). However, the rotors in the simulation and the experiment can only be aligned circumferentially to within +/- 6 N Δt degrees, and this leads to the small difference in phase.

For the signal reconstructed from Fourier components in Fig. 4, only the fundamental and first harmonic of the vane-passing frequency were used. Visually, this simplification appears to be adequate, but it is possible to show rigorously that that the 36E and 72E components are the most relevant using signal processing techniques. Parseval's theorem states that the integral of the power-spectral density of a signal over a range of frequencies yields the contribution of those frequencies to the signal mean-square (Ifeacher and Jervis, 1996). Consider Fig. 5(a) and 5(b), which are contour plots of the percentage of the signal variance obtained by integrating the power-spectral densities of time-resolved pressures at all grid points on the blade pressure and suction sides, respectively over the frequency range 34E-74E (1/4-wheel model). Also plotted on the figures are the locations of the Kulite static-pressure sensors. Note that the vane-passing and twice vane-passing frequencies account for over 90% of the predicted mean-square unsteadiness in static pressure over the entire blade surface. So, using the 36E and 72E frequencies only to reconstruct the experimental trace in Fig. 4(b) is adequate, and it is possible to restrict further comparisons of the 1/4-wheel and 1/18-wheel predictions to those frequencies.

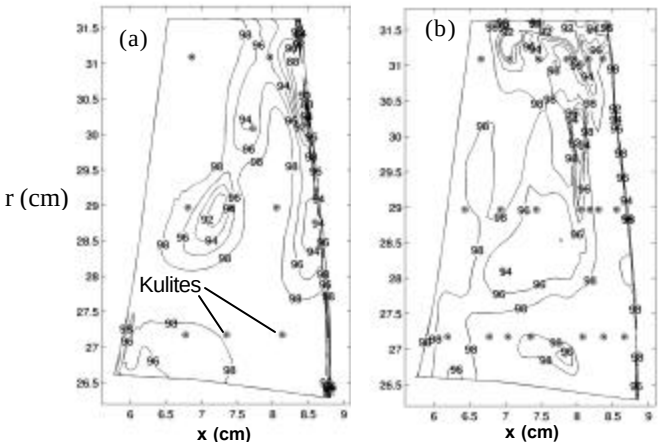

Figure 5. Over 90% of the predicted mean-square unsteadiness is contained in the frequency range from 34E-74E on both the (a) pressure and (b) suction sides.

In Fig. 6, measured and predicted DFT magnitudes on the pressure side of the blade are compared. The contour plots for the blade surfaces are percent difference values between the 1/4-wheel and 1/18-wheel simulations relative to the maximum magnitude of the predicted unsteadiness in the 1/4-wheel case at 36E and 72E. There are significant discrepancies in the DFT magnitudes between the two

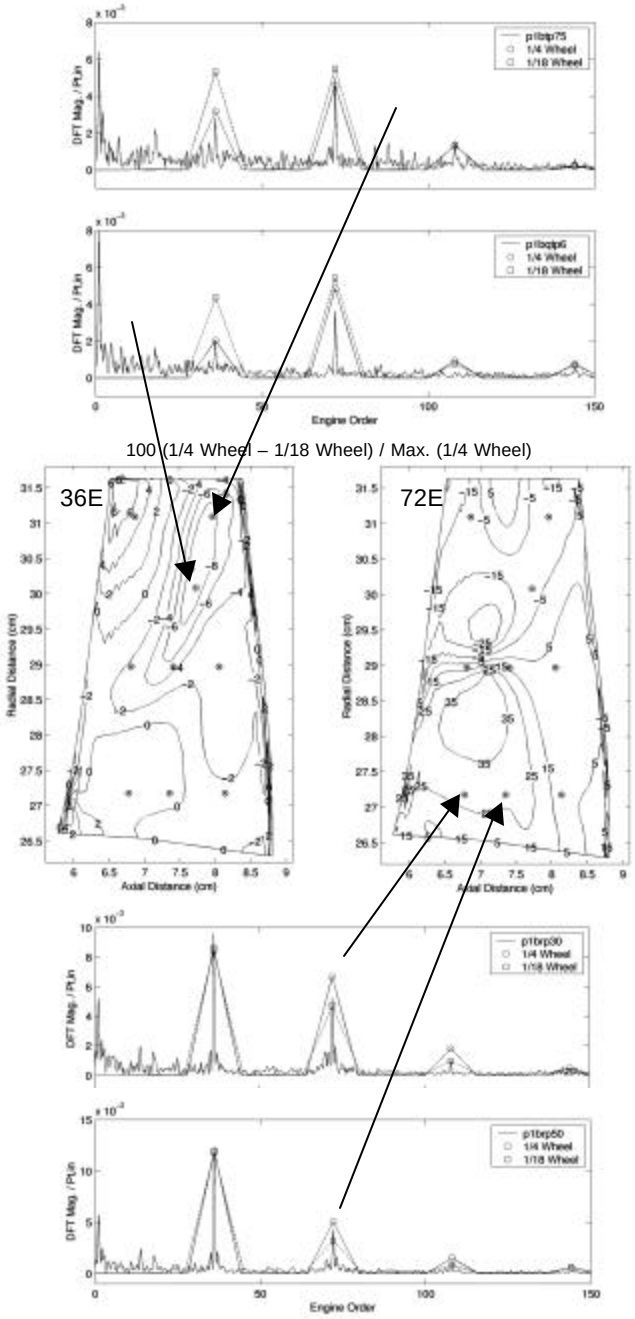

Figure 6. A comparison of measured and predicted DFT magnitudes for the 1B pressure side.

simulations at both frequencies. At 36E, the differences are most pronounced at the tip, with the 1/4-wheel simulation predicting greater unsteadiness forward of mid-chord and lesser aft than the 1/18-wheel prediction. However, the disparity between the two simulations is more apparent at 72E with the greater unsteadiness predicted near the root for the 1/4-wheel case and less near the tip than that of the 1/18-wheel prediction. The variations of DFT magnitude with engine order are plotted over a range including the fundamental vane-passing frequency and four harmonics for several sensor locations where the largest discrepancies between predictions are found. At 36E, the 1/4-wheel simulation better predicts the distributions of DFT magnitude over the pressure surface measured in the experiment both qualitatively and quantitatively. Also, the 1/4-wheel simulation is conservative with respect to the magnitude of fluctuations at 72E, whereas the 1/18-wheel prediction is anti-conservative. Overall, the 1/4-wheel simulation better represents the physics of the vane-blade interaction in the rig than the calculation in which airfoil scaling was used.

Figure 7 is organized similarly to Fig. 6. At the 36E frequency the absolute value of the percent difference in predicted magnitude was less than 4% over the entire surface of the blade where sensors were located. The 72E unsteadiness-levels are significantly greater near the root in the 1/4-wheel prediction forward of mid-chord. The distributions of DFT magnitude with engine order are plotted for several sensor locations where the largest discrepancies between the predictions are found. Again, the 1/4-wheel simulation is conservative with respect to the magnitude of fluctuations at 72E, whereas the 1/18-wheel prediction is anti-conservative.

The discrepancies in time-resolved blade loadings between the pre-test predictions mean that simulations involving airfoil scaling may result in under- or over-prediction of resonant stresses on excited blades, depending on the vibratory mode of interest. Worse still, when such an analysis is performed during the design process, design changes to alleviate a high level of predicted vibratory stress may in fact have the opposite of the intended effect if the sources of excitation are not well understood.

To visualize the mechanisms responsible here for the unsteadiness at each frequency, contour plots of the instantaneous pressure field in the blade passage are given in Fig. 8 for a number of time-steps from the 1/18-wheel prediction. Two sets of contour plots are shown, and these correspond to snapshots of the pressure field in the frame of reference of the moving blades. The fluctuating pressures plotted in the contour plots on the left and right have been notch filtered at 36E and 72E, respectively. Application of the narrow-band-pass filters allows visualization of the vane-blade interaction at each of the frequencies of interest in isolation.

Before filtering, the time-resolved pressures in the upstream vane-row were interpolated onto a grid that was fixed in the frame of reference of the blade row. This interpolation was applied only to the data plotted in Fig. 8, which was used only to visualize the 36E and 72E vane/blade interaction effects. As a consequence of the interpolation, it was possible to calculate the time-mean static pressure throughout the entire flow-field in the blade frame of reference and to subtract it from the instantaneous pressure. Thus the propagation of pressure waves across the interface was preserved. With the DC level removed, a digital finite-impulse response (FIR) filter that had an exactly linear phase-response in the pass-band was used to accentuate the fluctuations at the frequency of interest.

At each time-step depicted in Fig. 8, and for each of the contour plots at a given interval, the cross-passage shock wave is discernible to some degree in the blade passage. Note that no unsteady pressure fluctuations that propagate from the interaction with the upstream vane row penetrate that shock and continue downstream. Also note that there is some unsteadiness at both 36E and 72E which is propagating upstream to the trailing-edge region of the blade suction side. These pressure waves are generated by the reflection of the blade trailing-edge shock from the downstream vane row and transition duct. These

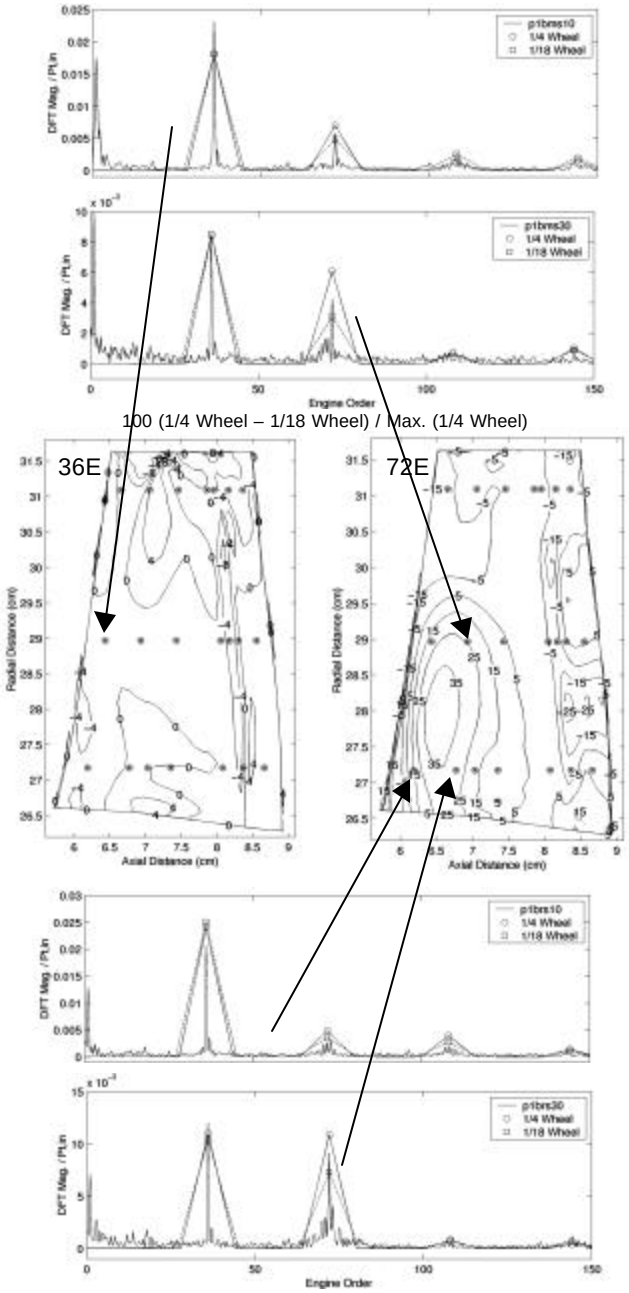

Figure 7. A comparison of measured and predicted DFT magnitudes for the 1B suction side.

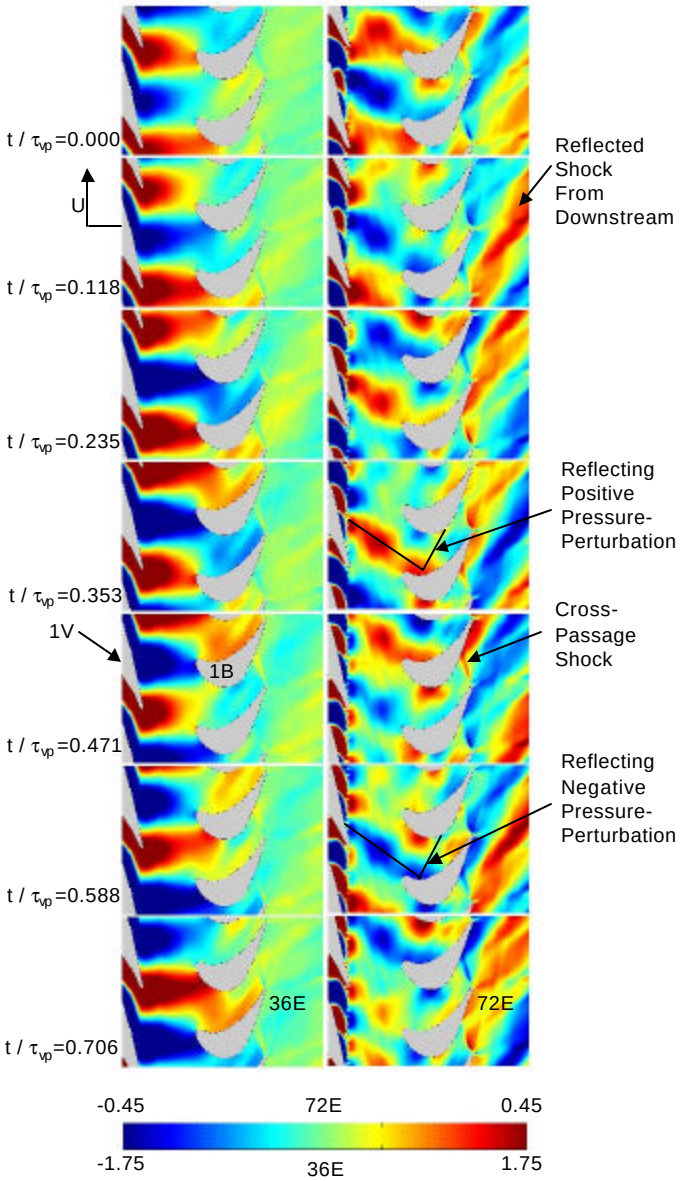

Figure 8. Instantaneous static-pressure contours in the blade frame of reference. The time-resolved pressures have been notch-filtered at 36E (left column) and 72E (right column) to visualize the unsteadiness due to those frequencies only.

waves do not propagate upstream of the cross-passage shock. Thus it may be concluded that the largest discrepancies between the simulations, which occur upstream of the cross-passage shock, must result from differences in the first-vane/blade interaction.

As the circumferential distortion in static pressure associated with the exit of each first-vane passage passes upstream of the rotor, the blades are subjected to alternating positive and negative pressure perturbations. These perturbations are either two or four in number depending upon whether 36E or 72E notch-filtered fluctuations are considered. These sets of perturbations are consequences of the waveform the circumferential distortion in static pressure takes at a given radius. The perturbations give rise to potential interactions that propagate and reflect through the blade row, creating complex interference patterns with each other and in turn interacting with wake events that are convecting with the local freestream. Such interference patterns are heavily dependent on the geometry of the blade passage. This is the reason that the 1/4-wheel and 1/18-wheel predictions, which represent small changes in the blade geometry from case to

case, yield different levels of unsteadiness on the blade surfaces, particularly at the 72E frequency where the interference pattern is more complex.

The first-vane/blade interaction is greater in an absolute sense than that of the blade/transition-duct/second vane as far as the blade is concerned. However, the latter interaction is of great importance downstream of the blade, and the interesting and complex moving-shock-interactions occurring in the transition duct and second vane as a consequence of the passage of the blade are the subject of a future study.

CONCLUSIONS

The effect of airfoil scaling on predictions of the time-resolved static pressure on the blade surface in a 1 and 1/2 stage transonic turbine has been assessed. Significant differences in the predicted first vane/ first blade potential interaction were found, and these manifested as discrepancies in amplitudes of unsteadiness on both the pressure and suction surfaces of the airfoil, particularly at twice vane-passing frequency. When no airfoil scaling was used and the true airfoil counts were modeled, the predicted levels of unsteadiness on the blade were in very good agreement with measurements in a short-duration turbine rig. Consequently, the code may be used with confidence both to predict forcing functions for resonant stress calculations and to discern the mechanics of such interactions in the future provided the geometry of interest is modeled accurately. The results presented here are also pertinent to the design of transonic turbines since time-resolved airfoil loadings are often predicted using CFD models employing scaled airfoils. Designers should take great care in using scaled results to reduce high levels of unsteadiness at multiples of the relevant passing frequency. Building on this investigation, a further study is to address the physics of the complex reflected-shock interaction between the blade, the transition duct, and the second vane.

ACKNOWLEDGEMENTS

The authors would like to express their gratitude to Mr. Ronald Takahashi of Pratt & Whitney. Mr. Takahashi performed the preliminary analyses that were used to decide the placement of sensors throughout the rig. Also, his experience with numerical simulation of unsteady flows and his advice were very valuable throughout this study. Mr. Jeff Barton at the OSU Gas Turbine Laboratory was instrumental in completing the experimental portion of the study, and his work was greatly appreciated.

REFERENCES

Busby, J. A., Davis, R. L., Dorney, D. J., Dunn, M. G., Haldeman, C. W., Jr., Abhari, R. S., Venable, B. L., and Delaney, R. A., 1998, "Influence of Vane-Blade Spacing on Transonic Turbine Stage Aerodynamics, Part II: Time-Resolved Data and Analysis", ASME 98-GT-482.

Davis, R. L., Shang, T., Buteau, J., and Ni, R. H., 1996, "Prediction of 3-D Unsteady Flow in Multi-Stage Turbomachinery Using an Implicit Dual Time-Step Approach," AIAA Paper No. 96-2565.

Dring, R. P., Joslyn, H. D., Hardin, L. W., and Wagner, J. H., 1982, "Turbine Rotor-Stator Interaction," ASME *Journal of Engineering for Power*, Vol. 104, pp. 729-742.

Dunham, J. and Meauze, G., 1998, "An AGARD Working Group Study of 3D Navier-Stokes Codes Applied to Single Turbomachinery Blade Rows," ASME Paper No. 98-GT-50.

Dunn, M. G., Moller, J. C., and Steele, R. C., 1989, "Operating Point Verification for a Large Shock Tunnel Test Facility," WRDC-TR-2027.

Dunn, M. G. and Haldeman, C. W., Jr., 1995, "Phase-Resolved Surface Pressure and Heat-Transfer Measurements on the Blade of a Two-Stage Turbine," ASME *Journal of Fluids Engineering*, Vol. 117, pp. 653-658.

Giles, M. B., 1990, "Stator/Rotor Interaction in a Transonic Turbine," AIAA *Journal of Propulsion and Power*, Vol. 6, pp. 621-627.

Hilbert, G. R., Ni, R. H., and Takahashi, R. K., 1997, "Forced-Response Prediction of Gas Turbine Rotor Blades," ASME Winter Annual Meeting.

Hilditch, M. A., Smith, G. C., and Singh, U. K., 1998, "Unsteady Flow in a Single Stage Turbine," ASME 98-GT-531.

Ifeachor, E. C. and Jervis, B. W., 1996, *Digital Signal Processing*, Addison-Wesley, New York.

Jones, T. V., Schultz, D. L., and Henley, A. D., 1973, "On the Flow in an Isentropic Light Piston Tunnel," ARC Report No. 34217, U.K.

Lax, P. D., and Wendroff, B., 1964, "Difference Schemes for Hyperbolic Equations with High Order Accuracy," *Communications on Pure and Applied Mechanics*, Vol. 17, pp. 381-398.

Ni, R. H., 1982, "A Multiple-Grid Scheme for Solving the Euler Equations," *AIAA Journal*, Vol. 20, No. 11, pp. 1565-1571.

Ni, R. H. and Bogoian, J. C., "Prediction of 3-D Multistage Turbine Flow Field Using a Multiple-Grid Euler Solver," AIAA Paper No. 89-0203.

Ni, R.H., "Advanced Modeling Techniques for New Commercial Engines," 1999, XIV ISOABE Conference, Florence, Italy, 5-10 September.

Rai, M. M., 1987, "Navier-Stokes Simulations of Rotor-Stator Interaction Using Patched and Overlaid Grids," AIAA *Journal of Propulsion and Power*, Vol. 3, pp. 387-396.

Rai, M. M. and Madavan, N. K., 1990, "Multi-Airfoil Navier-Stokes Simulations of Turbine Rotor-Stator Interaction," ASME *Journal of Turbomachinery*, Vol. 112, pp. 377-384.

Rao, K. V., Delaney, R.A., and Dunn, M.G., 1994, "Vane-Blade Interaction in a Transonic Turbine, Part 1: Aerodynamics," ASME *Journal of Propulsion and Power*, Vol. 10, No. 3, pp. 305-311.

Sharma, O. P., Pickett, G.F., and Ni, R.H., 1992, "Assessment of Unsteady Flows in Turbines," ASME *Journal of Turbomachinery*, Vol. 114, pp. 79-90.

Smith, M. C., and Kuethe, A. M., 1966, "Effects of Turbulence on Laminar Skin Friction and Heat Transfer," *Physics of Fluids*, Vol. 9, No. 12, pp. 2337-2344.

Tyler, J. M. and Sofrin, T. G., 1970, "Axial Flow Compressor Noise Studies," *SAE Transactions*, Vol. 70, pp. 309-332.